JOURNAL OF GEOPHYSICAL RESEARCH, VOL. 99, NO. A3, PAGES 4131–4141, MARCH 1, 1994

Fine structure of low-energy H^+ in the nightside auroral region

Chao Liu and J. D. Perez
Physics Department, Auburn University, Auburn, Alabama

T. E. Moore and C. R. Chappell
NASA Marshall Space Flight Center, Huntsville, Alabama

J. A. Slavin
NASA Goddard Space Flight Center, Greenbelt, Maryland

Low-energy H^+ data with 6-s resolution from the retarding ion mass spectrometer instrument on DE 1 have been analyzed to reveal the fine structure at middle altitudes of the nightside auroral region. A new method for deconvolving the energy-integrated count rate in the spin plane of the satellite has been used to derive the two-dimensional phase space density. A detailed analysis reveals an alternating conic-beam-conic pattern with the observed conics correlated with large earthward currents in the auroral region. The strong downward current (>1 $\mu A/m^2$(equivalent value at ionosphere)) provides a free energy source for the perpendicular ion heating, that generates the ion conics with energies from several eV to tens of eV. The bowl shape distribution of the low-energy H^+ is caused by the extended perpendicular heating. The strong correlation between conics and large downward currents suggests that the current-driven electrostatic ion cyclotron wave is an appropriate candidate for the transverse heating mechanism.

1. INTRODUCTION

During the last decade the phenomena of upflowing ions along the magnetic field line in the auroral zone and polar cap region have been extensively studied in order to understand the acceleration and transport processes [*Shelley and Collin*, 1991]. Now it is generally accepted that upward ion beams with energies above a keV are produced by large-scale parallel electric fields [*Reiff et al.*, 1988] and that conics are generated by the acceleration of ions perpendicular to the magnetic field [*Peterson et al.*, 1988, 1992]. A variety of candidates which may be responsible for ion transverse heating have been proposed to explain the complicated properties, such as the compositions, altitude dependence and morphologies [*Klumpar et al.*, 1984; *Retterer et al.*, 1987; *Horwitz*, 1986; *Borovsky*, 1984; *Moore et al.*, 1985, 1986]. However, the energization and transport processes of very low energy ionospheric ions to the hot magnetosphere are not fully understood. More detailed analyses are needed to distinguish the different models and free energy sources for a variety of conics.

The observations from the retarding ion mass spectrometer (RIMS) instrument on DE 1 have increased the knowledge of the plasma source for the magnetosphere [*Chappell et al.*, 1987]. The low-energy outflow observed in the polar region exhibits a significant content of heavy ions (typical O^+) with a transverse heating signature [*Lockwood et al.*, 1985; *Moore et al.*, 1986], that cannot be accounted for by the classical polar wind model. Such low-energy O^+ outflows are believed to originate from the dayside polar cap boundary or auroral zone, and the terms "upwelling ions" and "cleft ion fountain" are used to refer to these events and the source region respectively. Most analyses of RIMS data, however, have been integrated over several spins of the satellite and therefore have not been able to observe small-scale structure if it exists. Even though the nightside upflowing ions are a direct ionospheric source for the plasma sheet, the low-energy upflowing ions in the nightside auroral region have been given less attention. This is particularly true for the type of fine structure presented here.

Recent reports from the rocket TOPAZ 3 revealed the small-scale structure of transverse ion accelerations in the upper ionosphere, which are produced by the localized lower hybrid waves [*Arnoldy et al.*, 1992; *Vago et al.*, 1992]. At the mid-altitude auroral zone, low-energy particle measurements with high time resolution made by Exos D [*Miyake*, 1991] showed that field-aligned shifts of the bulk velocity of upflowing ions are well correlated with electron precipitation on a small scale, indicating that the shifts in the bulk velocity of the elevated conics are caused by acceleration due to parallel electric fields. An earlier relationship between ion perpendicular heating and field aligned current [*Cattel et al.*, 1980] and/or drift of thermal electrons [*Kintner and Gorney*, 1984] was not confirmed by the Exos D measurements. On the basis of observations from the Viking spacecraft, *Lundin et al.* [1987] suggested that ion conics are related to electrons in a more complicated way. Up to now, observations have been unable to show one-to-one correspondence between currents and conics on a small scale.

This paper examines the low-energy H^+ data of RIMS from DE 1 on a small scale. It presents the fine structure of low-energy ion outflows at mid-altitude in the nightside auroral region and discusses the free energy sources for the low-energy ion conics. In section 2 the analysis technique is briefly described, and the observations are presented. In section 3 we show phase space densities with high time resolution (6-s). An alternating

Paper number 93JA01989.
0148-0227/94/93JA-01989$05.00

conic-beam-conic pattern and a correlation with the small-scale variation of strong downward current are found. The bowl shape of some ion phase space densities and the current-driven electrostatic ion cyclotron waves are discussed in section 4. Conclusions are presented in section 5.

2. OBSERVATION AND ANALYSIS TECHNIQUE

The data analyzed in this paper was collected by the DE 1 satellite which is in polar orbit with an apogee of 4.65 R_E and a perigee of 1.1 R_E. Even though the results from several instruments onboard DE 1 are referred too, we focus on the retarding ion mass spectrometer (RIMS) [*Chappell* et al., 1981]. The RIMS consists of three sensor heads: the radial head which lies in a spin plane, and the $+Z$ head and $-Z$ head which are parallel and antiparallel to the spin axis, respectively. The radial head with a mass spectrometer and a retarding potential analyzer (RPA) makes it possible to derive the phase space density of each species in the plane that contains the magnetic field. The spin period of the radial head is the same as that of the satellite, which is about, but slightly larger than 6 s (59.4 deg/s). Examining summary data plots from day 280, 1981, when the first useful data was obtained, through day 329, 1981, when the radial head RPA failed, we found several examples of alternating conic-beam-conic patterns. We analyze in detail two of those days, October 24, 1981 (day 297) and October 14, 1981 (day 287), when DE 1 passed through the nightside auroral region (Figure 1). These were chosen because they are particularly active times so that the characteristics we present are most clear. The significant events on day 297 are identified as E1, E2, E3, and E4. Event E1 contains field aligned ion beams and conics that are associated with a different mechanism than the one presented in this paper. As shown later in this section, events E2 and E4 have alternating conic-beam-conics associated with strong downward flowing currents. The event E3 shows ion beams with large velocities perpendicular to the magnetic field. On day 287, the events are identified as G1, G2, and G3. They are related to the corresponding events on day 297, that is, E1, E2, and E3. There is no event on day 287 corresponding to E4. The events E2, E4, and G2 are analyzed in this paper. Events E1, E3, G1, and G3 will be the subject of future papers because the physical mechanism acting in these cases is entirely different.

The bottom part of Plate 1 shows the RIMS spectrogram of H^+, which plots spin angle against universal time (UT) between 1320 and 1354 on day 297, October 24. The event E1 extends from 1325 to 1332 UT; E2 from 1339 to 1342 UT; E3 from 1344 to 1348 UT; and E4 from 1351 to 1353 UT. Additional parameters describing the location of the satellite are also presented, that is, magnetic local time (MLT), geocentric distance (RE), magnetic latitude (MLAT), and the McIlwain L shell value (L). During this time, DE 1 traveled equatorward from the polar cap into the plasmasphere. During E2, there are small-scale time variations of the two morphologies: conic and beam. Even though the instrument shut down for about 3 min, 1348 to 1351 UT, another alternating conic-beam-conic pattern was observed at E4.

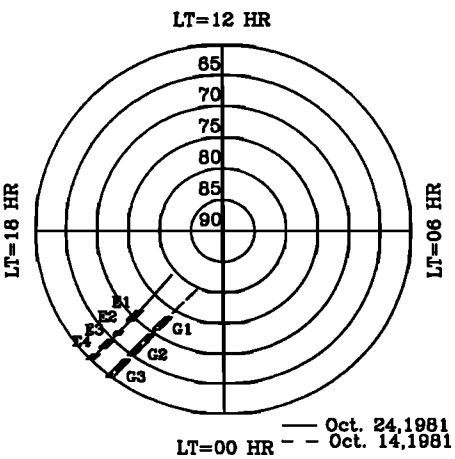

Fig. 1. DE 1 orbit and the events of low-energy ion outflow are plotted on the coordinate system of invariant latitude versus magnetic local time (northern hemisphere).

Shown at the top of Plate 1 are the field-aligned current derived from the magnetic field data from the instrument MAG-A on DE 1 [*Marshall et al.*, 1991] and the parallel potential determined from the electron and ion measurements from the high-altitude plasma instrument (HAPI) on DE 1 using the method of *Gurgiolo and Burch* [1988]. The event E2 is associated with an inverted-V electron precipitation event that occurs between E2 and E3. High energy ion beams associated with the inverted-V event are observed by the HAPI instrument [*Marshall et al.*, 1988]. What we see in E2 is the appearance of low- energy ion outflow at the regional boundary and the edges of an inverted-V electron precipitation event where the high-energy component is absent. Event E4 is near the plasmasphere boundary and is not associated with an inverted-V event. Both events E2 and E4, however, are colocated with regions of strong downward current.

A complete interpretation of the physical mechanism responsible for the events E2 and E4 requires that we look at the phase space density. To determine the phase space density, a deconvolution must be performed.

A full RPA sweep of the RIMS instrument from 0 to 50 eV requires 0.5 s and covers an angle range of about 30 deg when the radial head sensor rotates in its spin plane. A typical data set is shown in Plate 2. Data points from each of the 12 full RPA sweeps during a single satellite spin are shown in the boxes placed in the appropriate angular range around the center box. For analysis purposes the uncertainty in the measured data is taken to be the square root of the counts per sample. In the center, the counts per sample when the RPA voltage is zero are plotted. For ease of display, the maximum value is normalized to unity. This center box provides an initial qualitative picture of the ion distribution, that is, it can indicate whether a beam or conic is present. In the center box the direction of the magnetic field and the direction of plasma velocity due to the satellite motion (RAM) are indicated. It is important to recall that each data point, corresponding to each RPA voltage, is actually at a different angle. During each of the 12 complete RPA sweeps, the RPA voltage goes from 0 to 50 eV twice, but in different steps. The first set of values are shown by circles, the second by plus signs. Therefore we do not have complete energy information at any single angle nor do we have complete angle information at any specific energy. In order to extract the localized plasma structure with sharp angular variations, a new technique of two-dimensional deconvolution of the energy-integrated count rate in the spin plane has been used [*Perez et al.*, 1993]. As an example of this technique, curves of the fit to the data given in Plate 2 are also shown there.

This technique based on a method developed by *Wahba* [1990] consists of seeking the plasma ion distribution function f by solving the variational equation,

$$\delta(\chi^2 + \beta Z + \lambda P) = 0,$$

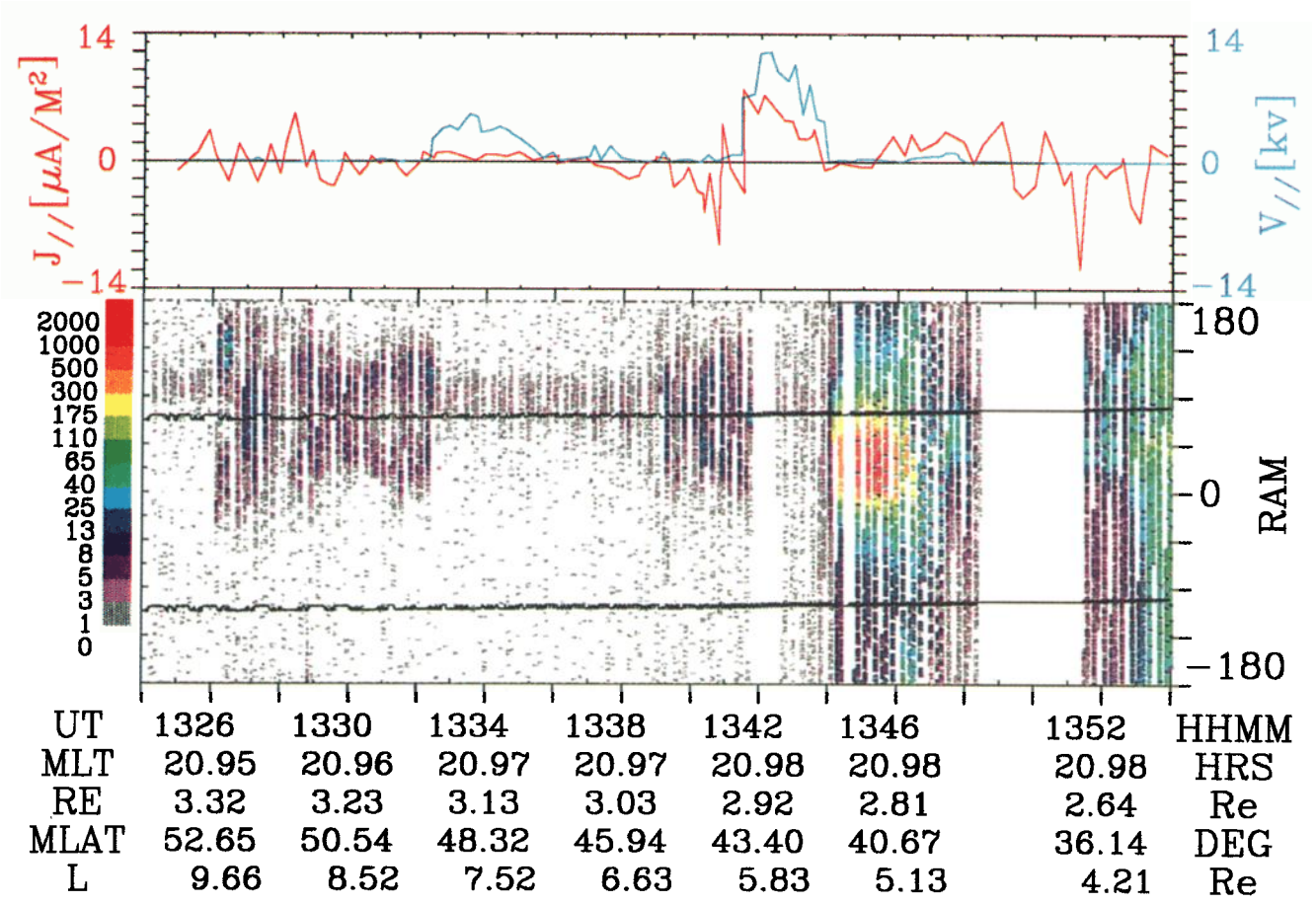

Plate 1. DE 1 retarding ion mass spectrometer (RIMS) spin spectrogram for H^+ (bottom). On the top panel the field-aligned current and parallel potential taken from Figure 1 of *Marshall et al.* [1991].

where χ^2 is the weighted sum of the square of the difference between the measured count rate and the count rate calculated from the hypothesized f, P is a penalty function, λ is a free parameter which balances the fit of the data against the smoothness of the deconvolved f, Z is a constraint condition $I(E=0) = 0$, and β is a undetermined Lagrange multiplier. As *Wahba* [1990] suggested, the best value of λ is chosen by the method of generalized cross validation (GCV). Expansion of the unknown intensity by a tensor product of cubic B-splines [*de Boor*, 1978], converts the variation equation into a system of linear equations. By solving for the expansion coefficients, the phase space density can be obtained.

An important question regarding the deconvolution method is the uncertainty in the resulting phase space density contours. The answer to this question is complicated by the properties of the bicubic splines [*de Boor*, 1978] used to expand the unknown function. For a fixed choice of the breakpoints and knots that define the basis set of splines, estimates of the statistical error in the expansion coefficients can be made in the standard way [*Press*, 1989]. This, however, does not address the issue of uncertainty introduced due to the choice of expansion functions, that is, by changes in the breakpoints or knots. Extensive tests of the deconvolution method on a variety of types of RIMS data [*Perez et al.*, 1993] as well as other types of data [*Fisher and Perez*, 1991] show quite clearly that the shape, the features, and the moments of the deconvolved phase space densities are a true reflection of the data and the calibrated response of the instrument.

3. ALTERNATING CONIC-BEAM-CONIC PATTERN

In this section the alternating conic-beam-conic patterns, as well as their phase space densities for each 6 s interval, are discussed in detail. On day 297 in 1981 the RIMS instrument operated in the mode alternating between the low-mass channel and the high-mass channel. This results in 8-s gaps in the H^+ data from the low-mass channel, but the event E2 of day 297 still shows clearly the small-scale structures. On the left part of Figure 2, count rates per sample with zero RPA potential from the radial head of RIMS at a series of times, noted at the top of Figures 2*a* through 2*h*, are plotted against the pitch angle for event E2. These plots are the same format as the center box of Plate 2. The corresponding deconvolved phase space densities are shown in the right part of Figure 2. A beam appears first at the time 1339:10 UT (Figure 2*a*). Then one wing of a conic is observed at 1339:28 UT (Figure 2*b*), suggesting an even smaller-scale inhomogeneity of the plasma during this 6-s period. Following it, we show the two beams at 1339:42 UT (Figure 2*c*) and 1340 UT (Figure 2*d*) and two conics at 1340:16 UT (Figure 2*e*) and 1340:32 UT (Figure 2*f*). It is interesting that the conic angle in the Figure 2*f* depends on the energy, and its distribution resembles a "bowl". For the Figure 2*g*, the two morphologies are mixed with the right part as one wing of the conic and the left part as beam, which again shows the

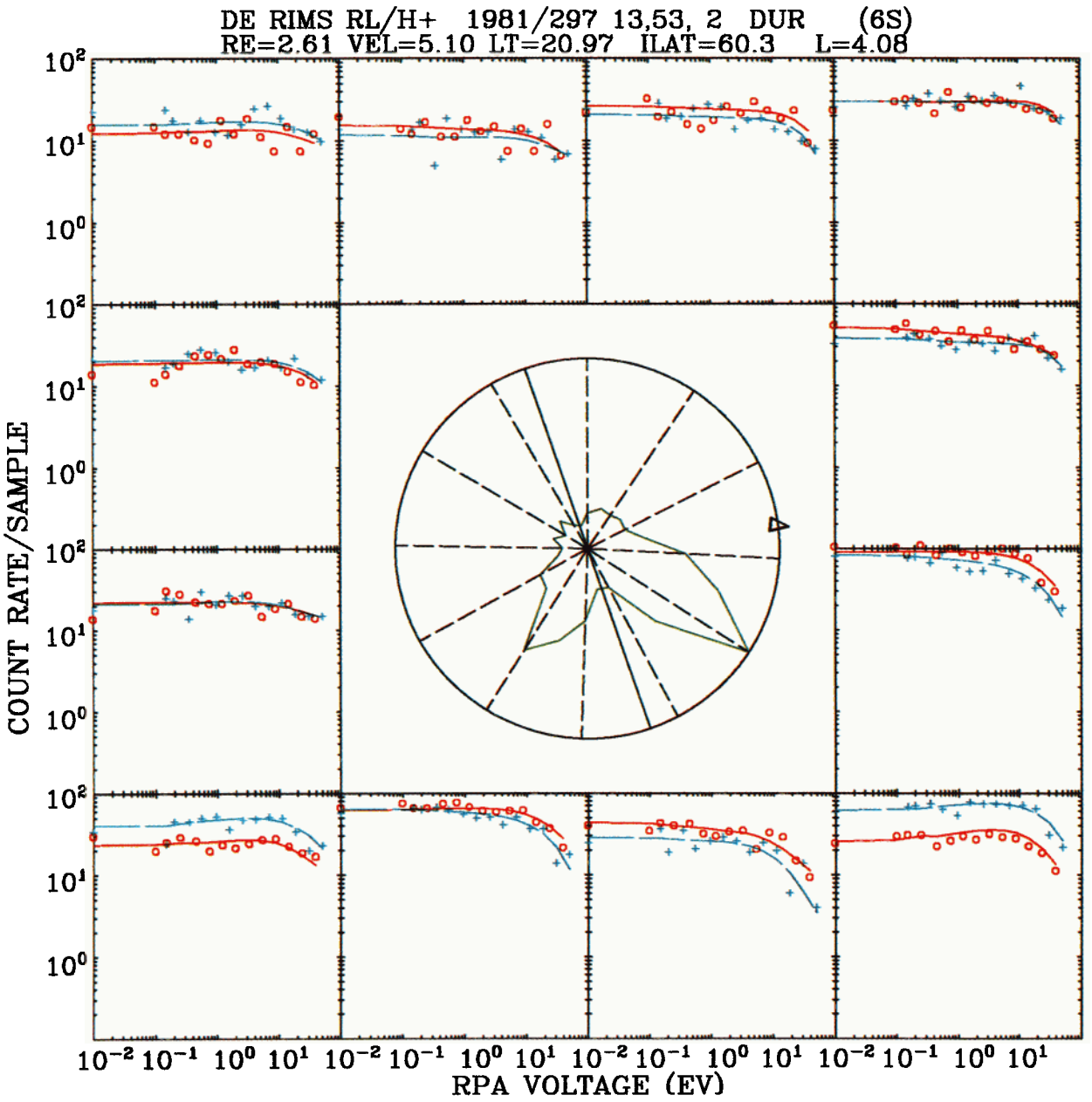

Plate 2. H+ data from one spin of RIMS radial head and the fitting curves. The angle arrangement is indicated in the central panel.

variation of plasma structure during the 6 s. In Figure 2*h*, there is a conic with field-aligned ions of high energy. In all cases, whether the distribution is conical or beamlike, there is significant outflow from the ionosphere to the magnetosphere, and the distribution is highly non-Maxwellian.

The universal times, at which the distribution is identified as a beam or a conic, are plotted along with the current obtained by *Marshall et al.* [1991] in Plate 3. The current density from MAG-A [*Farthing et al.*, 1981] data has been adjusted to the equivalent value at the ionosphere by considering the convergence of the flux tube with altitude. The alternating conic-beam-conic pattern exhibited in E2 is strongly correlated with the downward current region. When the downward current exceeds ~1 $\mu A/m^2$, a conic distribution is observed. Otherwise we have a beam-like distribution of low-energy ions. Near the inverted-V electron precipitation, the ion conic is mixed with the beam that is accelerated by the U-shape parallel potential (Figure 2*h*).

Another example of the small-scale structure is given in Figure 3 for E4 of day 297, in which a similar fine structure in the low-energy ions is shown. Again they exhibit the correlation with the downward currents (Plate 3). The average density, velocity, and energy for both E2 and E4 are shown in Table 1.

While there are many other examples of alternating conic-beam-conic patterns in the RIMS data, current data is not available for all of them. To show that the events analyzed in detail in this paper are not isolated cases, we present data from October 14, 1981 (day 287). The event G2 occurs during a large geomagnetic storm as indicated by the $K_p = 8$ during the three hour period from 0000 to 0300 UT. The count rates and phase space densities for day 287 are shown in Figure 4. The current and the location of

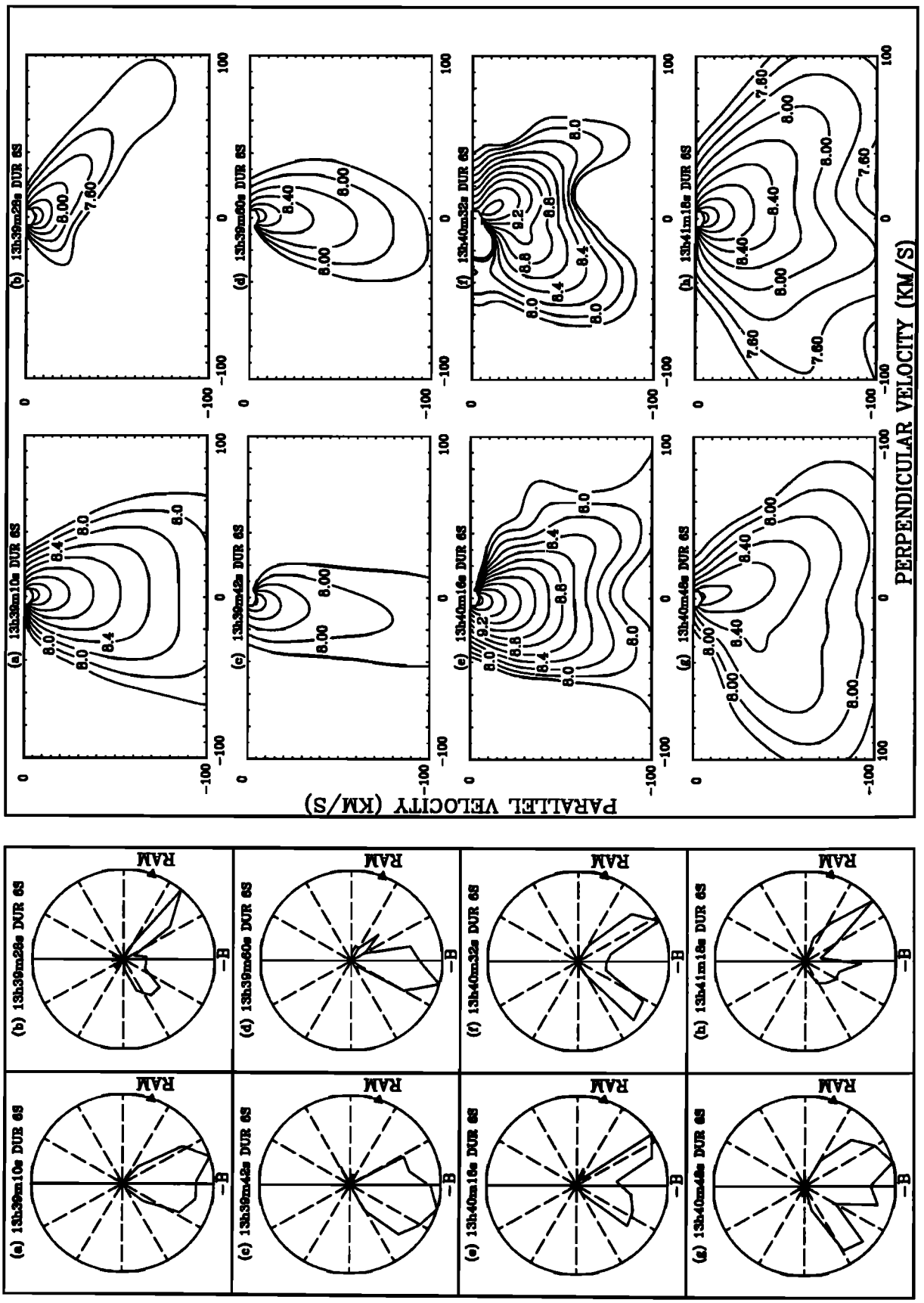

Fig. 2. (Left) Normalized counts per sample (Vrps=0) versus pitch angle for E2 of day 297. (Right) Contour plots of the phase space density.

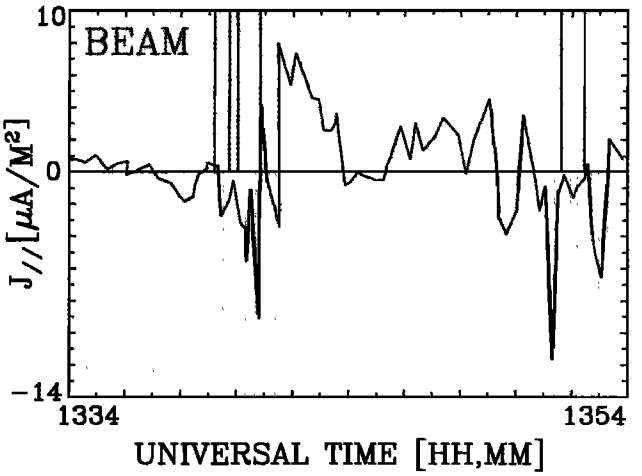

Plate 3. Current and location of beams and conics for day 297, events E2 and E4.

the conics and beams are plotted in Plate 4. Again, we see the strong correlation between large downward current and conics.

4. DISCUSSION

The conical distribution in phase space is generally interpreted as the result of ion mirror motion in the diverging magnetic field after localized perpendicular heating at a lower altitude. The conservation of the ion energy and magnetic moment during the mirror motion makes the pitch angle independent of the energy as the particle moves up along the field line. The particle pitch angle α can be written in the following form:

$$\sin^2\alpha = \frac{v_\perp^2}{v^2} = \frac{\mu|\vec{B}|}{E} ,$$

where v is the particle velocity, $v_\perp$ the component perpendicular to B, the magnetic field, and E is the total energy of the particle. Since the quantity μ/E remains constant along the mirror motion trajectory, the pitch angle remains the same for all particles that started with an identical pitch angle. In contrast, ion heating causes the pitch angle to change with the particle energy, that is,

$$d(\sin^2\alpha) = \left(\frac{E_\parallel}{E^2}\right)_{B,E_\parallel} dE_\perp - \left(\frac{E_\perp}{E^2}\right)_{B,E_\perp} dE_\parallel + \left(\frac{\mu}{E}\right)_{E_\parallel,E_\perp} dB .$$

If perpendicular ion heating occurs not at a single altitude but rather over an extended region, the first term shows that the pitch angle as observed at a higher altitude becomes energy-dependent. If there is no parallel heating and the energy input of perpendicular heating depends on energy such that $dE_\perp \propto E^\gamma$ and $\gamma<2$, the larger the energy, the pitch angle moves closer to the magnetic field line. This produces the bowl shape distribution exhibited in Figure 2*f*. In contrast, if in addition to localized perpendicular heating, there is parallel acceleration as suggested by the bimodal mechanism of *Klumpar et al.* [1984], the larger energy has the wider pitch angle. The completely different energy-dependent characteristics of the pitch angle can be used as a tool to distinguish the dominant mechanism for the formation of conics. The bowl shape distribution observed here is a clear indicator of extended perpendicular heating for this conic.

The strong correlation on small spatial scales between the downward currents and low-energy conics suggests clearly that the downward current is the free energy source for the transverse ion heating, that generates conics with energies from several eV to tens of eV (Table 1). The current-driven electrostatic ion cyclotron instability has been invoked as a mechanism for ion transverse heating for a long time. As *Kindel and Kennel* [1971]discussed, the electrostatic ion cyclotron wave (EIC) can easily be destabilized by a field-aligned current. The EIC waves then produce the perpendicular heating of the particles. The critical electron drift velocity associated with this instability is an increasing function of the ion temperature (their Figure 1). Thus heating can saturate the instability by raising the ion temperature, so that the downward current no longer exceeds the critical value. The transverse heating causes the temperature to be anisotropic, which should be included in a detailed calculation of the critical velocity [*Lee*, 1972]. The simulation done by *Ganguli and Palmadesso* [1987] suggests that an electron drift velocity corresponding to a downward current of 0.65 $\mu A/m^2$ is above the threshold for EIC waves. This is consistent with the critical downward current ~1 $\mu A/m^2$ inferred here as shown in Plates 3 and 4.

Recently, a one-dimensional simulation of the downward current region was done by *Brown et al.* [1991], which showed conical distributions of H^+ with energy of a few electron volts that are indicative of extended perpendicular heating. Even though the observation and the calculation are not at exactly the same altitude, a comparison of the hydrogen distribution from their simulation and from the RIMS instrument is of interest. The main features of the bowl distribution for H^+ shown in their Figure 3 are in good agreement with the phase space distribution at 1340:32 UT with an altitude 1.97 R_E (Figure 2*f*).

The bowl distribution observed here corresponds to the largest downward current in the pattern, which makes the ion perpendicular heating occur over the most extended region of altitude. An estimate of the field-aligned length of the heating region is obtained from the pitch angle at about 50 eV (~145°) and at low energies (~90°). On this basis the source region extends from about 1 R_E to near the satellite altitude of 2 R_E. When the downward current is lower than the value at the time in Figure 2*f*, the transverse acceleration occurs only in a small region at an altitude below the satellite. In this case, what is observed is a superposition of unheated background plasma and a part of a

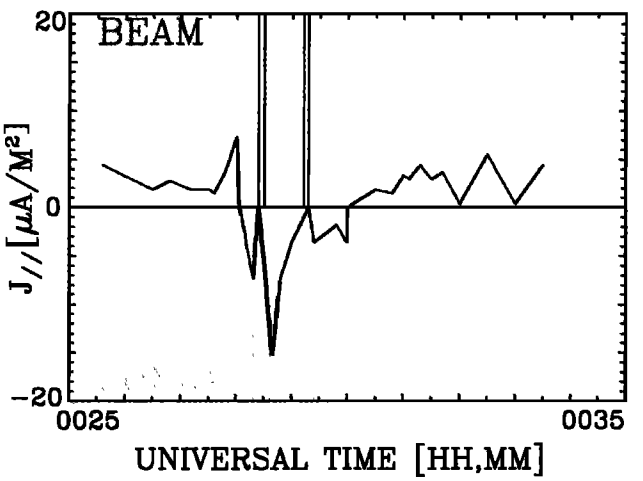

Plate 4. Current and location of beams and conics for day 287.

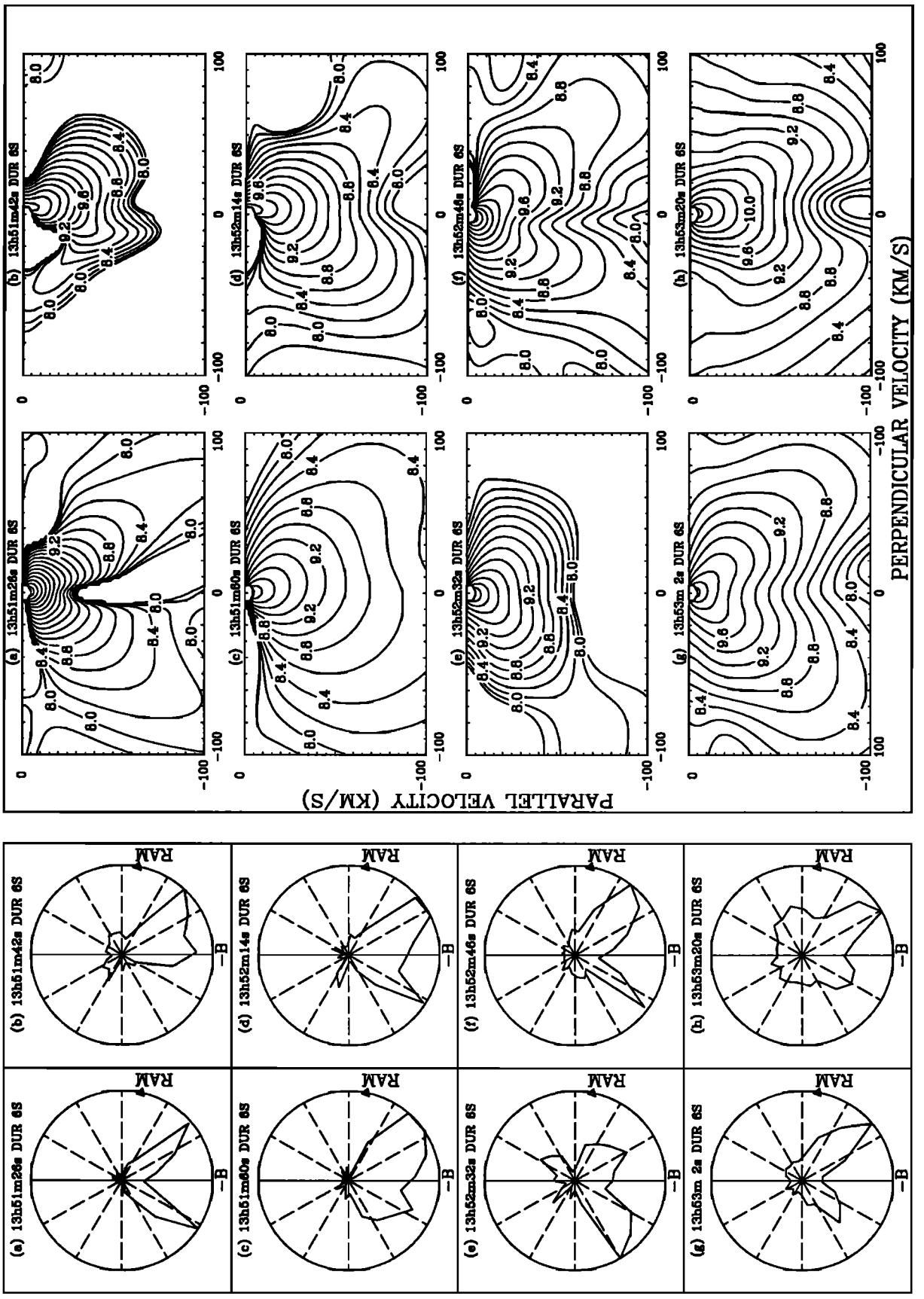

Fig. 3. (Left) Normalized counts per sample (V_{PB}=0) versus pitch angle for E4 of day 297. (Right) Contour plots of the phase space density.

TABLE 1. Density, Velocity, and Energy for Events E2 and E4 on October 24, 1991, Determined From Retarding Ion Mass Spectrometer Data

UT	Type	n, cm^{-3}	$v_{//}$, km/s	$v_{\perp}$, km/s	$T_{//}$, eV	$T_{\perp}$, eV
			Event E2			
1339:10	beam	0.18	-37.1	2.0	7.6	5.7
1339:28	conic	0.04	-24.7	7.9	9.4	17.1
1339:42	beam	0.06	-37.5	-7.5	11.6	6.9
1340:00	beam	0.07	-39.9	2.0	8.5	6.4
1340:16	conic	0.32	-26.9	-1.7	5.1	4.2
1340:32	conic	0.36	-29.8	4.5	4.1	8.5
1340:48	beam	0.23	-40.1	-2.1	7.8	11.9
1341:20	conic	0.17	-33.9	5.1	6.8	11.2
			Event E4			
1351:26	conic	1.72	-10.5	1.6	2.5	2.7
1351:42	beam	0.85	-11.3	7.7	3.7	2.7
1352:00	conic	1.01	-29.6	5.2	8.8	10.2
1352:14	conic	0.87	-22.6	0.4	7.0	7.0
1352:32	beam	0.78	-11.5	-0.2	5.4	5.3
1352:46	conic	2.30	-15.9	4.2	9.0	9.8
1353:02	conic	2.70	-16.7	4.2	9.3	12.4
1352:20	conic	4.98	-10.2	4.3	10.0	10.0

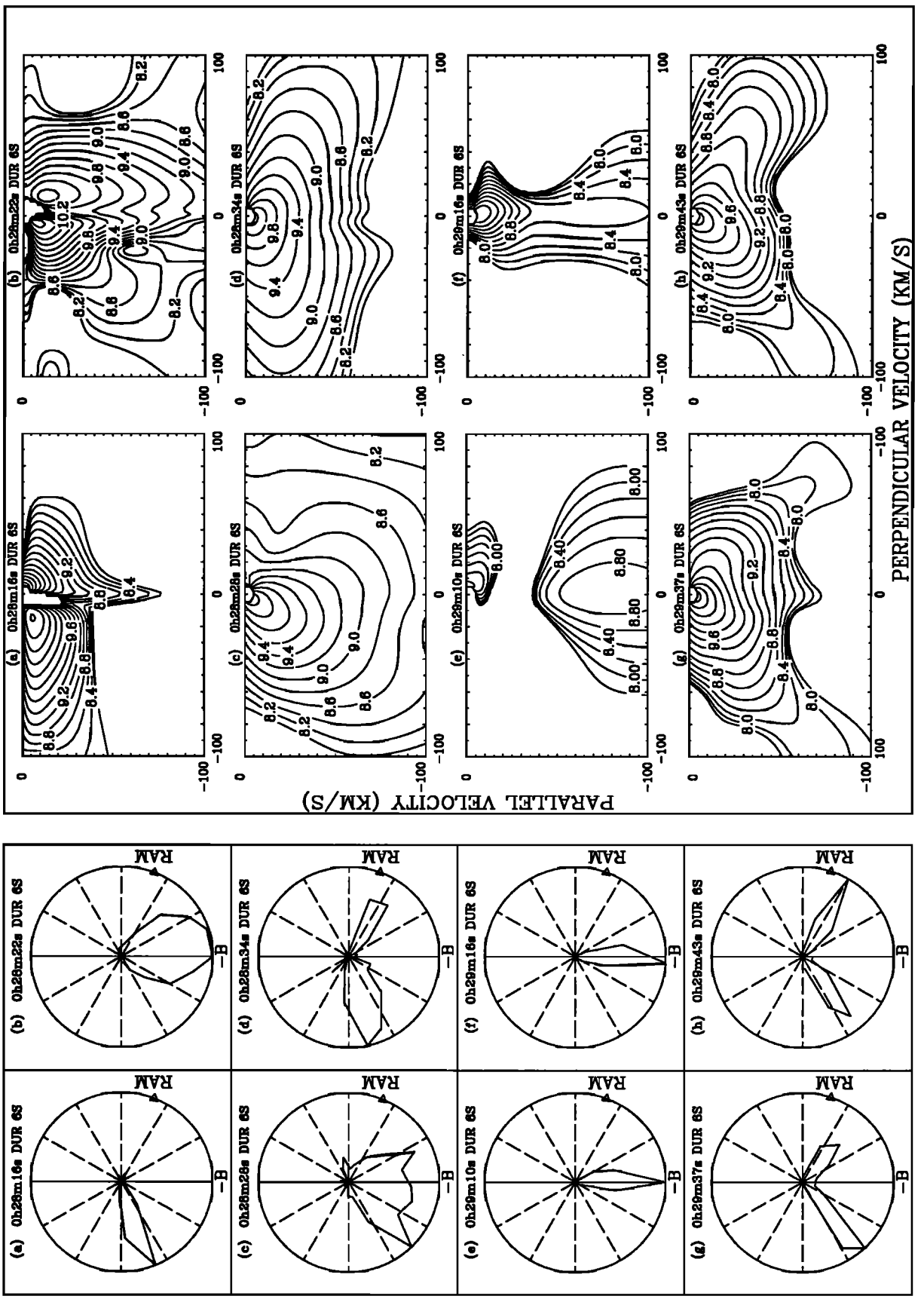

Fig. 4. (Left) Normalized counts per sample (V_{rpa}=0) versus pitch angle for G2 of day 287. (Right) Contour plots of the phase space density.

conical distribution that has the appropriate velocity to reach the observed altitude at the observed time (Figures 4*b* and 2*e*.)

On the basis of the quasi-linear theory, *Dusenbery and Lyons* [1981] showed that the resonant interaction of upgoing thermal ions with thermal electrons can generate ion conic distributions only in the downward current region and that ion conics should not occur simultaneously with the inverted-V keV electron precipitation. This is consistent with the fact that we see ion conics correlated with strong downward currents and that we see no low-energy ion conics in the region between events E2 and E3.

5. CONCLUSION

The fine structure of the low-energy ions at mid-altitude in the nightside auroral region, that is, the alternating conic-beam-conic pattern, is correlated with the downward current. The strong downward current provides a free energy source for the perpendicular ion heating, which generates the ion conics with energies from several eV to tens of eV. Comparison between the observations presented here and previous theoretical models and simulations suggests that the current-driven electrostatic ion cyclotron wave is an appropriate candidate for the transverse heating mechanism. A bowl-shaped distribution of low-energy H^+ is interpreted as being caused by extended perpendicular heating. Further theoretical work and simulations are necessary in order to fully explain the laminar structure exhibited in the conic-beam-conic pattern and the small-scale variation of downward current [*Marshall et al.*, 1988] along with the formation of the fine structure shown in the discrete aurora [*Lysak*, 1992].

Acknowledgments. The authors thank Barbara Giles, Marshall Space Flight Center, for her assistance in accessing the RIMS data. The work reported here was supported by the NASA JOVE program under contract NAG8-147.

The Editor thanks W. K. Peterson and another referee for their assistance in evaluating this paper.

REFERENCES

Arnoldy, R. L., K. A. Lynch, P. M. Kintner, J. Vago, S. Chesney, T. E. Moore, and C. J. Pollock, Burst of transverse ion acceleration at rocket altitudes, Geophys. Res. Lett., 19, 413, 1992.

Borovsky, J. E., The production of ion conics by oblique double layers, *J. Geophys. Res., 89,* 2251, 1984.

Brown, G. B., G. R. Wilson, J. L. Horwitz, and D. L. Gallagher 'Self-consistent' production of ion conics on return current region Auroral field lines: A Time-dependent, Semi-kinetic model, *Geophys. Res. Lett., 18,* 1841, 1991.

Cattel, C., R. Lysak, R. B. Torbert, and F. S. Mozer, Observations of differences between regions of current flowing into and out of the ionosphere, *Geophys. Res. Lett., 6,* 621, 1980.

Chappell, C. R., S. A. Fields, C. R. Baugher, J. H. Hoffman, W. B. Hanson, W. W. Wright, H. D. Hammock, G. R. Carignan, and A. F. Nagy, The retarding ion mass spectrometer on Dynamics explorer-A, *Space Sci. Instrum., 5,* 477, 1981.

Chappell, C. R., T. E. Moore, and J. H. Waite, Jr., The ionosphere as a fully adequate source of plasma for the earth's magnetosphere, *J. Geophys. Res., 92,* 5896, 1987.

de Boor, Carl, *A Practical Guide to Splines,* Springer-Verlag, New York, 1978.

Dusenbery, P. B., and L R. Lyons, Generation of ion-conic distribution by upgoing ionospheric electrons, *J. Geophys. Res., 86,* 7627, 1981.

Farthing, W. H., M. Sugiura, B. G. Ledley, and L. J. Cahill, Jr., Magnetic Field Observations on DE-A and -B, *Space Sci. Instrum. 5,* 551, 1981.

Fisher, T. R., and J. D. Perez, The use of spline expansions and regularization in the unfolding of data from spaceborne sensors, *Proc. SPIE Int. Soc. Opt. Eng., 1479,* 212, 1991.

Ganguli, S. B., and P. J. Palmadesso, Plasma transport in the auroral return current region, *J. Geophys. Res., 92,* 8673, 1987.

Gurgiolo, C., and J. L. Burch, Simulation of electron distributions within auroral acceleration regions, *J. Geophys. Res., 93,* 3989, 1988.

Horwitz, J. L., Velocity filter mechanism for ion bow distributions (Bimodal conics), *J. Geophys. Res., 91,* 4513, 1986.

Kindel, J. M., and C. F. Kennel, Topside current instabilities, *J. Geophys. Res., 76,* 3055, 1971.

Kintner, P. M., and D. J. Gorney, A search for the plasma processes associated with perpendicular ion heating, *J. Geophys. Res., 89,* 937, 1984.

Klumpar, D. M., W. K. Peterson, and E. G. Shelley, Direct evidence for two-stage (Bimodal) acceleration of ionospheric ions, *J. Geophys. Res., 89,* 10,799, 1984.

Lee, K. F., Ion cyclotron instability in current carrying plasma with anisotropic temperature, *J. Plasma Phys., 8,* 379, 1972.

Lockwood, M., J. H. Waite, Jr., T. E. Moore, J. F. E. Johnson, and C. R. Chappell, A new source of suprathermal O^+ ions near the dayside polar cap boundary, *J. Geophys. Res., 90,* 4099, 1985.

Lundin, R., L. Eliason, B. Hultqvist, and K. Stasiewics, Plasma energization on auroral field lines as observed by the Viking spacecraft, *Geophys. Res. Lett., 14,* 443, 1987.

Lysak, R. L., Electron acceleration in the Alfven wave model of auroral arcs, in *Source Transport, Energization, and Loss of Magnetospheric Plasmas,* 3rd Huntsville Workshop on Magnetosphere/Ionosphere Plasma Model, edited by J. L. Horwitz and T. E. Moore, Guntersville, AL, 1992.

Marshall, J. A., J. L. Burch, J. R. Kan, and J. A. Slavin, DE 1 observations of return current regions in the nightside auroral oval, *J. Geophys. Res., 93,* 14542, 1988.

Marshall, J. A., J. L. Burch, J. R. Kan, P. H. Reiff, and J. A. Slavin, Sources of field-aligned currents in the auroral plasma, *Geophys. Res. Lett., 18,* 45, 1991.

Miyake, W. T., Mukai, N. Kaya, and H. Fukunish, Exos-D observations of upflowing ion conics with high time resolution, *Geophys. Res. Lett., 18,* 341, 1991.

Moore, T. E., C. R. Chappell, M. Lockwood, and J. H. Waite., Jr., Superthermal ion signatures of auroral acceleration processes, *J. Geophys. Res., 90,* 1611,1985.

Moore, T. E., M. Lockwood, M. O. Chandler, J. H. Waite, Jr., C. R. Chappell, A. Persoon, and M. Sugiura, Upwelling O^+ ion source characteristics, *J. Geophys. Res., 91,* 7019, 1986.

Perez, J. D., Chao Liu, L. Lawson, T. E. Moore, and C. R. Chappell, A new technique for deconvolution of data from instruments that make integral measurements, e.g. RIMS on DE-1, *Annales Geophysicae 11,* 889, 1993 .

Press, W. H., B. P. Flannery, S. A. Teukolsky, and W. T. Vetterling, *Numerical Recipes,* Cambridge University Press, New York, 1989.

Peterson, W. K., E. G. Shelley, S. A. Boardsen, D. A. Gurnett, B. G. Ledley, M. Sugiura, T. E. Moore, and J. H. Waite, Transverse ion energization and low-frequency plasma waves in the mid-altitude auroral zone: a case study, *J. Geophys. Res., 93* , 11,405 , 1988.

Peterson, W. K., H. L. Collin, M. F. Doherty, and C. M. Bjorklund, O^+ and He^+ restricted and extended (Bi-modal) ion conic distribution, *Geophys. Res. Lett., 19,* 1439, 1992.

Reiff, P. H., H. L. Collin, J. D. Craven, J. L. Burch, J. D. Winningham, E. G. Shelley, L. A. Frank, and M. A. Friedman, Determination of auroral electrostatic potential using high- and low-altitude particle distributions, *J. Geophys. Res., 93,* 7441, 1988.

Retterer, J. M., T. Chang, and G. B. Crew, J. R. Jasperse, and J. D. Winningham, Monte Caro modeling of Ionospheric oxygen acceleration by cyclotron resonance with broad-band electromagnetic turbulence, *Phys. Rev. Lett., 59,* 148, 1987.

Shelley, E. G., and H. L. Collin, Auroral ion acceleration and its relationship to ion composition, in *Auroral Physics,* edited by Ching-I. Meng, M. J. Rycroft, and L. A. Frank, p. 129, Cambrige, University Press, New York, 1991.

Vago, J. L., P. M. Kintner, S. W. Chesney, R. L. Arnoldy, K. A. Lynch, C. J. Pollock, and T. E. Moore, Transverse ion acceleration by localized

lower hybrid waves in the topside auroral ionosphere, *J. Geophys. Res., 97*, 16,935, 1992.

Wahba, G., *Spline Models for Observational Data*, Society for Industrial and Applied Mathematics, Philadelphia, Pa., 1990.

C. R. Chappell, Associate Director for Science/Code DS01, NASA Marshall Space Flight Center, Huntsville, AL 35812.

C. Liu and J. D. Perez, Physics Department, Auburn University, Auburn, AL 36849.

T. E. Moore, Space Science Laboratory/Code ES53, NASA Marshall Space Flight Center, Huntsville, AL 35812.

J. A. Slavin, NASA Goddard Space Flight Center, Greenbelt, MD 20771.

(Received March 8, 1993;
Revised March 25, 1993;
Accepted July 8, 1993.)